

Short-Term Parafoveal Cone Loss Despite Preserved Ellipsoid Zone in Rod Cone Dystrophy

Danial Roshandel^{1,2}, Rachael C. Heath Jeffery^{1,2}, Jason Charng^{1,2},
Danuta M. Sampson³, Samuel McLenachan^{1,2}, David A. Mackey^{1,2}, and
Fred K. Chen^{1,2,4,5}

¹ Centre for Ophthalmology and Visual Science, The University of Western Australia, Perth, Western Australia, Australia

² Ocular Tissue Engineering Laboratory, Lions Eye Institute, Nedlands, Western Australia, Australia

³ Surrey Biophotonics, Centre for Vision, Speech and Signal Processing and School of Biosciences and Medicine, The University of Surrey, Guildford, UK

⁴ Department of Ophthalmology, Royal Perth Hospital, Perth, Western Australia, Australia

⁵ Department of Ophthalmology, Perth Children's Hospital, Nedlands, Western Australia, Australia

Correspondence: Fred K. Chen, Ocular Tissue Engineering Laboratory, Lions Eye Institute, 2 Verdun Street, Nedlands WA, Australia. e-mail: fredchen@lei.org.au

Received: June 21, 2021

Accepted: November 15, 2021

Published: December 14, 2021

Citation: Roshandel D, Heath Jeffery RC, Charng J, Sampson DM, McLenachan S, Mackey DA, Chen FK. Short-term parafoveal cone loss despite preserved ellipsoid zone in rod cone dystrophy. *Transl Vis Sci Technol.* 2021;10(14):11, <https://doi.org/10.1167/tvst.10.14.11>

Purpose: Rod–cone dystrophy (RCD) is characterized by centripetal loss of rod followed by cone photoreceptors. In this prospective, observational cohort, we used flood-illumination adaptive optics (AO) imaging to investigate parafoveal cone loss in regions with preserved ellipsoid zone (EZ) in patients with RCD.

Methods: Eight patients with RCD and 10 age-matched healthy controls underwent spectral-domain optical coherence tomography and AO imaging. The RCD cohort underwent a follow-up examination after 6 months. Cone density (CD) and intercone distance (ICD) measurements were performed at 2° temporal from the fovea. Baseline CD and ICD values were compared between the control and patient groups, and longitudinal changes were calculated in the patient group. Residual EZ span in patients was measured in horizontal foveal B-scans.

Results: Between the control and patient groups, there was no significant difference in the baseline CD (2094 vs. 1750 cells/deg², respectively; $P = 0.09$) and ICD (1.46 vs. 1.62 arcmin, respectively; $P = 0.08$). Mean CD declined by 198 cells/deg² (−11.3%; $P < 0.01$), and mean ICD increased by 0.09 arcmin (+5.6%; $P = 0.01$) at the 6-month follow-up in the patient group. Mean baseline and follow-up residual EZ spans in the six patients with EZ defect were 3189 μm and 3065 μm, respectively (−3.9%; $P = 0.08$).

Conclusions: AO imaging detected significant parafoveal cone loss over 6-month follow-up even in regions with preserved EZ. Further studies to refine AO imaging protocol and validate cone metrics as a structural endpoint in early RCD are warranted.

Translational Relevance: CD and ICD may change prior to EZ span shortening in RCD.

Introduction

Rod–cone dystrophy (RCD) is the most common form of inherited retinal disease (IRD) and is characterized by generalized and progressive rod photoreceptor cell loss followed by cone photoreceptor dysfunction and degeneration. Functional and structural endpoints have been used for estimating the disease progression rate in natural history studies¹ and interventional clinical trials.² Thickness and span of the

outer retinal layers have been widely used as structural endpoints in RCD trials.³ The reduction in the length of the residual ellipsoid zone (EZ) span on spectral-domain optical coherence tomography (SD-OCT) has been shown to be a reliable measure of disease progression, and it correlates with retinal function decline.^{4,5} EZ span and area decline at a rate of approximately 4% to 10% and up to 13% per year, respectively, in patients with various types of RCD.^{5–7} Therefore, a clinically meaningful change in the EZ span may be detected over a period of 1 to 2 years.^{4,8} However, EZ

span serving as an endpoint is not feasible in early-stage RCD when the transitional zone is outside the imaging field.

Adaptive optics (AO) retinal imaging is a relatively new technology that enables *in vivo* imaging of the cone photoreceptors. The rtx1 (Imagine Eyes, Orsay, France) is a flood-illuminated ophthalmoscope (FIO) and the only commercially available AO retinal camera. Compared with the custom-built AO scanning laser ophthalmoscopes (AOSLOs), rtx1 has a wider imaging field with lower axial and transverse resolution.⁹ Both techniques, FIO and SLO, have been used to measure cone density (CD) and intercone distance (ICD) at different retinal eccentricities in normal individuals^{10–12} and a range of retinal pathologies, including RCD.^{13–15} In patients with RCD, a normal cone mosaic may be observed within the area of preserved EZ, which progresses to an irregular cone mosaic with decreased CD and increased ICD outside the transition zone where there is outer retinal atrophy.¹⁴ Using the rtx1 camera, a profound reduction in CD and an increase in ICD at the transitional zone between preserved and degenerated outer retinal layers were reported in two patients with RCD compared with five healthy subjects.¹⁶ Gale et al.^{17,18} studied the repeatability of CD measurements using the rtx1 camera in 10 patients with RCD caused by diverse genetic mutations. The coefficient of repeatability (CoR), defined as the threshold below which the test–retest difference lies 95% of the time if there was no difference, of CD at 2° to 5° eccentricities ranged between 2464 and 3514 cells/mm², which was comparable to their age-matched healthy controls investigated in a previous study. However, the study by Gale et al. was limited by localization of the foveal center based on the preferred retinal locus. In addition, they used custom software for automated cone detection without manual adjustment, which may overestimate CD by falsely detecting debris as cones.¹⁷ Therefore, it remains to be determined if the rtx1 AO camera can detect changes in CD and ICD in parafoveal regions that have yet to be invaded by the transitional zone. Therefore, the aim of this prospective proof-of-concept study was to investigate the ability of rtx1 AO imaging to detect parafoveal CD and ICD changes in areas with preserved EZ within a 6-month interval in patients with RCD.

Patients and Methods

Participants

Patients were recruited prospectively for multimodal imaging as part of the Western Australian Retinal

Degeneration study. Inclusion criteria for selection of AO images for analysis in this study were patients with RCD who were 18 to 65 years of age, with stable foveal fixation, best-corrected visual acuity (BCVA) equal to or better than 20/40, and two sets of AO images acquired 6 months apart with sufficient image quality for cone counting. Exclusion criteria included history of ocular surgery, co-existing retinal disease, significant cataract or other media opacity, nystagmus, cystoid macular edema (CME), epiretinal membrane (ERM), or a history of using systemic medications with known photoreceptor toxicity. An experienced inherited retinal disease specialist (FKC) confirmed the clinical diagnosis of RCD in all patients based on history, examination, and electroretinography. Healthy controls 18 to 65 years of age with normal BCVA and ocular examination were also recruited prospectively using the same imaging protocol. The study protocol was approved by the Human Ethics Committee of the Office of Research Enterprise, The University of Western Australia (RA/4/1/7916, 2021/ET000151 and RA/4/1/7226), and adhered to the tenets of the Declaration of Helsinki. Informed written consent was obtained from all participants.

Clinical Evaluation

All patients underwent comprehensive eye examinations, including visual acuity testing, slit-lamp examination, Goldmann applanation tonometry, and dilated fundus examination. BCVA was measured using the Early Treatment Diabetic Retinopathy Study (ETDRS) chart at a distance of 4 m using the standard protocol,¹⁹ and both ETDRS letter score and Snellen equivalent are reported. Autorefractometry (Ark1 Autorefractor and Keratometer; Nidek, Gamagori, Japan) and optical biometry (IOL Master; Carl Zeiss Meditec, Dublin, CA) were performed at the baseline visits. Ultra-widefield color fundus photography and green-light autofluorescence (AF) imaging (California; Optos, Dunfermline, UK), as well as short-wavelength (excitation $\lambda = 488$ nm) and near-infrared (excitation $\lambda = 887$ nm) fundus AF imaging (HRA2; Heidelberg Engineering, Heidelberg, Germany), were performed in the patient group at baseline examination. SD-OCT (Spectralis; Heidelberg Engineering) and AOFIO imaging (rtx1; Imagine Eyes, Orsay, France) were performed at baseline in both groups and after 6 months in the patient group. For all participants, only the right eye was enrolled in this study.

Imaging Protocols and Localization

Foveal-centered macular volumetric scans (30° × 25° scan field, 61 horizontal B-scans separated by

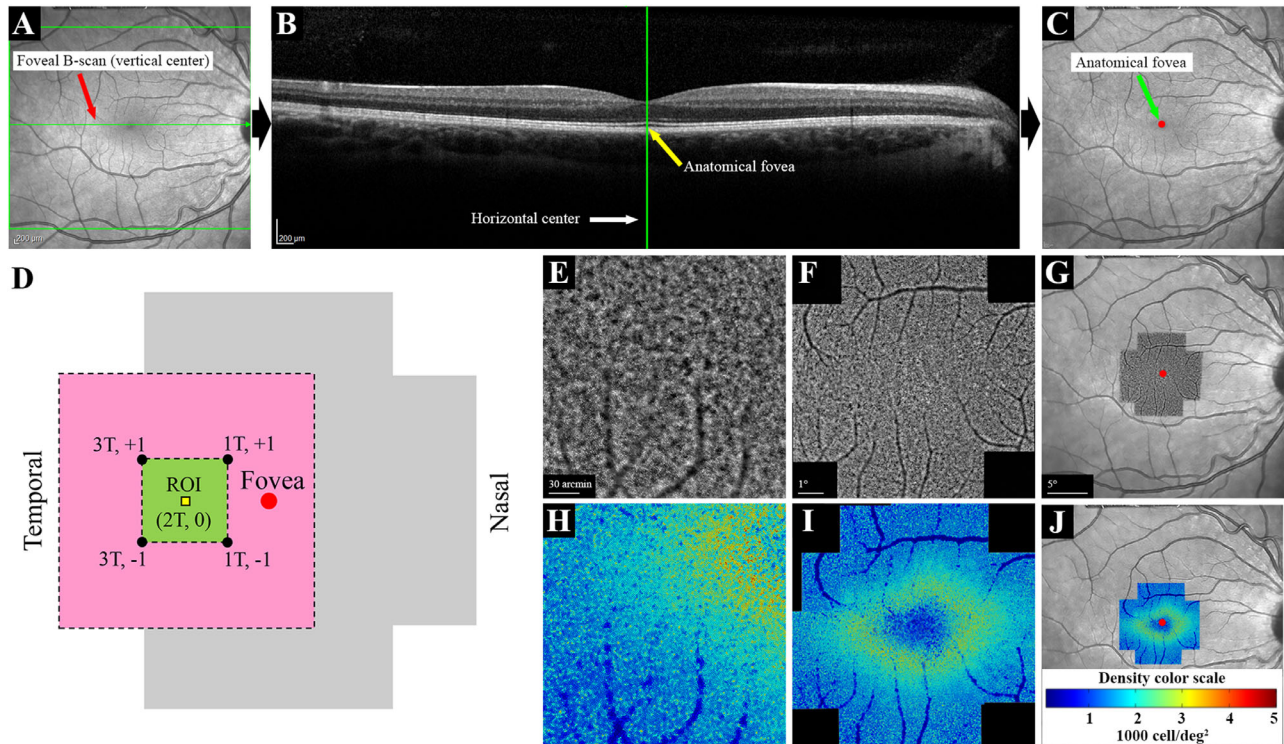


Figure 1. Procedures used for image acquisition, montage and marking the foveal center in a normal eye. Vertical (A) and horizontal (B) centers of the high-resolution IR image were located using the HEYEX software, and the foveal center was marked on the IR image (C). The AO imaging protocol included 12 overlapping $4^\circ \times 4^\circ$ image frames covering the central 10° (D). Fovea, region of interest (ROI), and x, y coordinates (degrees from the fovea) of the four overlapping image frames are shown. The pink area ($6^\circ \times 6^\circ$) shows the area covered by the four overlapping image frames, and the green area ($2^\circ \times 2^\circ$) shows the area shared by these image frames. The ROI ($80 \mu\text{m} \times 80 \mu\text{m}$) was located on the horizontal meridian, 2° temporal to the fovea. Individual AO image frames (E) were stitched together to create an AO montage (F). The AO montage was overlaid on the center-marked IR image, and the foveal center was marked on the AO montage (G). The same procedure was performed for the analyzed AO images to create cone density maps (H–J). The color code for the density map is shown in (J). T, temporal; +, superior; –, inferior.

$130 \mu\text{m}$) and accompanying high-resolution infrared (IR) image were used for marking the anatomical foveal center defined as the center of the foveal pit using the manufacturer software (HEYEX 1.9.14.0; Heidelberg Engineering) in all eyes (Figs. 1A–1C). This fovea-marked IR image was used for locating the foveal center on AO image montages (see below). In addition, horizontal EZ spans were measured on the foveal B-scans using the measurement tool provided in the HEYEX software.

AO imaging was performed after pupil dilation using 1% tropicamide and 2.5% phenylephrine eye drops. All imaging sessions were performed under dim light condition without dark adaptation. Manufacturer software (AOImage 3.0) was used for image acquisition, and photoreceptor mode was selected. The focus plane was set to $+40 \mu\text{m}$ to $+100 \mu\text{m}$ (corresponding to $40\text{--}100 \mu\text{m}$ above the retinal pigment epithelium). A series of $4^\circ \times 4^\circ$ images with 2° overlap, covering the central 10° , were taken of each eye at each examination (Fig. 1D). Each $4^\circ \times 4^\circ$ image frame was reconstructed

from up to 40 images acquired during 4 seconds (10 frames per second) that were able to be aligned and averaged using the internal software to increase the signal-to-noise ratio. Final image frames were exported and stitched together using the MosaicJ plug-in for ImageJ (National Institutes of Health, Bethesda, MD) (Figs. 1E, 1F). The resultant AO montage was overlaid on the center-marked IR image by matching the large vessels using Photoshop CC 2015 (Adobe Systems, San Jose, CA), and the center of the AO montage was marked (Fig. 1G).

We performed cone analysis at 2° eccentricity, at which the peak CD was reported using the rtx1 camera.²⁰ Also, the EZ was intact and a cone mosaic could be detected in all patients at the temporal 2° location in our cohort. The region of interest (ROI; 2° temporal) was shared by four temporal image frames with approximately equal distance to the image center (Fig. 2). The temporal 2° was found and marked on the center-marked AO montage and used for image analysis and cone counting (see below). Follow-up

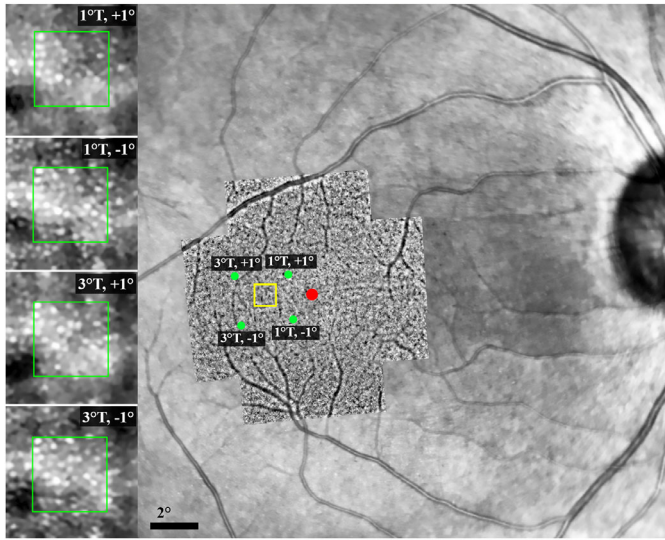


Figure 2. Location of the ROI on the AO montage overlaid on the IR image. The *red spot* shows the foveal center, and the *yellow box* shows the approximate location of the ROI (2° temporal to the foveal center along the horizontal meridian). *Green dots* show the center of each of the four image frames. Note that the distance of the ROI from the image frame centers is approximately the same for all image frames, although there is a mild rotation in the AO image compared with the background IR image. Magnified images on the *left side* represent the cone mosaic and precise alignment of the ROI (located within the *yellow box*) in the overlapping image frames. *Green boxes* show the dimensions of the sampling window (80 μm \times 80 μm). T, temporal; +, superior; -, inferior.

imaging was performed using a similar protocol. The same ROI was marked on follow-up examinations after alignment using the internal software followed by careful manual adjustment. All images were visually examined to ensure accurate alignment and adequate image quality. Images with undetectable cone mosaic or notable mosaic distortion compared with other corresponding image frames were excluded from the final analysis.

Image Analysis and Cone Counting

All image analyses and cone counting were performed using AODetect 3.0 (Imagine Eyes), which is an automated cone detection and analysis software based on MATLAB (MathWorks, Natick, MA) with the option of manual adjustment. Cones were marked in an 80 \times 80- μm window, and cone mosaic parameters including CD and ICD were calculated and reported in metric (cells/ mm^2 and μm) and angular (cells/ deg^2 and arcmin) units (Supplementary Fig. S1). Metric values were calculated and adjusted to the axial length of each patient. For each eye, the ROI was located on the first recorded baseline image frame in the AODetect software, and the sampling window

was placed on the closest location that was free from large vessels. The same location was found on the other three image frames of the same imaging session and all image frames of the follow-up examination. Because the image frames were overlapping, the ROI was captured four times by four partially overlapping image frames. All measurements were performed at the same ROI (i.e., 2° temporal to the fovea) on the four image frames. After running the image analysis by the software, marked cones were double checked and adjusted if required by an experienced grader (DR). The angular and metric CD and ICD values were recorded and used for subsequent statistical analyses. Data obtained from the two image frames with the highest CD and lowest ICD values were used to calculate intra-session CoR. Inter-session CoR values in the patient group were calculated using values obtained from the same coordinates after a 6-month interval. The image frame with the highest CD and lowest ICD values was used for comparing baseline mean CD and ICD values between the control and patient groups. Also, the highest CD and lowest ICD values from both visits were used for longitudinal analysis in the patient group. In addition, we used the older version of AODetect software (version 0.1-beta) that enables segmentation and analysis of the entire 4° \times 4° image frame and created a montage of the CD heat map in a healthy control (Figs. 1H–1J) and selected patients. Although the heat map generated using this method can be useful for detecting patterns of cone loss, this analysis was not used for CD measurements, as the sampling window was extremely large.

Statistical Analysis

Visual acuities were converted to logarithm of minimum angle of resolution (logMAR) units for statistical analysis. All data were recorded in SPSS Statistics 23 (IBM, Chicago, IL), and appropriate statistics were applied after testing for normality. The Shapiro–Wilk test for normality showed normal distributions of baseline CD and ICD values in all image frames in both groups, as well as in the follow-up examination of the patient group. Hence, the independent samples *t*-test was used to compare mean baseline CD and ICD values between control and patient groups, and the paired-samples *t*-test was used to compare mean CD and ICD values at 6 months with those at baseline. The CoR for CD and ICD was calculated as previously described.²¹ Briefly, average within-subject variance was calculated, and the square root of the average variance, which is equal to within-subject standard deviation (S_w), was multiplied by 2.77

Table 1. Demographics and Baseline Clinical Features of the Eight Patients

ID	Sex	Age (y)	Onset (y)	BCVA ^a	SE (D)	AL (mm)	Lens	Inheritance
1	M	20	AS	79 (20/25)	−1.25	24.33	Clear	AD
2	M	38	24 ^b	84 (20/20)	+1.00	22.50	Clear	AR
3	F	55	20 ^b	80 (20/25)	+3.00	21.84	Mild PSCC	AR
4	F	37	AS	85 (20/20)	−2.00	24.07	Clear	AR
5	F	42	34 ^c	88 (20/20)	−8.25	27.71	Clear	Simplex
6	F	49	10 ^c	80 (20/25)	+0.50	23.69	Clear	Simplex
7	M	22	14 ^b	69 (20/40)	−0.50	23.80	Mild PSCC	Simplex
8	F	46	38 ^c	84 (20/20)	+0.75	22.46	Clear	Simplex

AL, axial length; AD, autosomal dominant; AR, autosomal recessive; AS, asymptomatic; PSCC, posterior subcapsular cataract; RP, retinitis pigmentosa; SE, spherical equivalent.

^aETDRS letters at 4 m. Snellen equivalents are shown in parentheses.

^bNyctalopia.

^cVisual field constriction.

Table 2. Mean, SD, and Range of Baseline Clinical Features in the Control and Patient Groups

	Control (<i>n</i> = 10)	Patient (<i>n</i> = 8)	<i>P</i> ^a
Gender (M:F), <i>n</i>	5:5	3:5	—
Age (y), mean ± SD (range)	37 ± 13 (21 to 54)	39 ± 12 (20 to 55)	0.72
SE (D), mean ± SD (range)	−0.86 ± 1.79 (+1.25 to −4.75)	−0.84 ± 3.36 (+3.00 to −8.25)	0.99
AL (mm), mean ± SD (range)	24.17 ± 0.78 (22.86 to 25.40)	23.80 ± 1.81 (21.84 to 27.71)	0.60
BCVA (logMAR), mean ± SD (range)	−0.16 ± 0.09 (−0.24 to 0.06)	0.08 ± 0.12 (−0.06 to 0.32)	<0.01

^aIndependent samples *t*-test.

(derived from $1.96 \times \sqrt{2}$). Confidence intervals (CIs) for CoR values were calculated as follows: 95% CI = $1.96 \times S_w / (\sqrt{2n(m-1)})$, where *n* is the number of subjects and *m* is the number of observations. Bland–Altman plots were used to determine the relationships between test–retest differences and mean values for both CD and ICD. *P* < 0.05 was considered statistically significant.

Results

Patient Characteristics

We evaluated 220 patients with IRDs for eligibility for this study. Among 153 patients with RCD, 122 were excluded from the study for meeting one or more exclusion criteria. AO imaging was performed in the remaining 31 patients, among whom 17 were excluded due to lack of follow-up imaging and six were excluded due to a follow-up interval longer than 6 months (Supplementary Fig. S2). Eight patients with RCD (three males) with successful baseline AO imaging and at least 6-month follow-ups were enrolled

in the final analysis. The mean ± SD age at baseline examination was 39 ± 12 years (range, 20–55). Two patients were asymptomatic, and the age of onset of symptoms in the remaining six patients was 23 ± 11 years (range, 10–38) (Table 1). There was no significant difference in age, spherical equivalent, or axial length between the patient and control groups (Table 2). EZ constriction was detected in six patients with a baseline residual span of 3189 ± 1416 μm (range, 1392–5558). The nasal and temporal ends of the EZ line extended beyond the imaging field in the remaining two patients. Ultra-widefield AF showed a complete or incomplete macular hyperautofluorescent ring in six patients (Supplementary Fig. S3).

Repeatability

All image frames with adequate image quality were analyzed, and CD and ICD values were recorded. Two patients had only two available image frames at the 6-month follow-up. Overall, four of 40 images in the control group (10%), five of 28 images in the patient group at baseline (18%), and two of 28 images in the patient group at the 6-month follow-up (7%) were

Table 3. Mean, SD, and Range of CD and Intra-Session CoR in Control and Patient Groups in Angular and Metric Units

	Control (<i>n</i> = 10)	Patient (<i>n</i> = 8)	
		Baseline	6 Months
Mean CD, ^a cells/deg ² (cells/mm ²)			
Mean	2044 (24,122)	1661 (20,601)	1468 (18,320)
SD	173 (3203)	496 (6886)	513 (7039)
Minimum	1830 (20,182)	1120 (10,809)	901 (8311)
Maximum	2309 (28,770)	2306 (27,983)	2110 (25,315)
Test-retest difference, cells/deg ² (cells/mm ²) ^a			
Mean	38 (438)	84 (980)	96 (1290)
SD	122 (1513)	239 (2900)	265 (3196)
Minimum	1 (14)	25 (221)	5 (60)
Maximum	228 (2867)	578 (6839)	593 (7028)
CoR, cells/deg ² (cells/mm ²)	239 (2940)	468 (5649)	521 (6377)
CoR 95% CI, cells/deg ² (cells/mm ²)	±37 (±465)	±83 (±999)	±92 (±1128)

^aMeasurement using the two image frames with the highest CD.

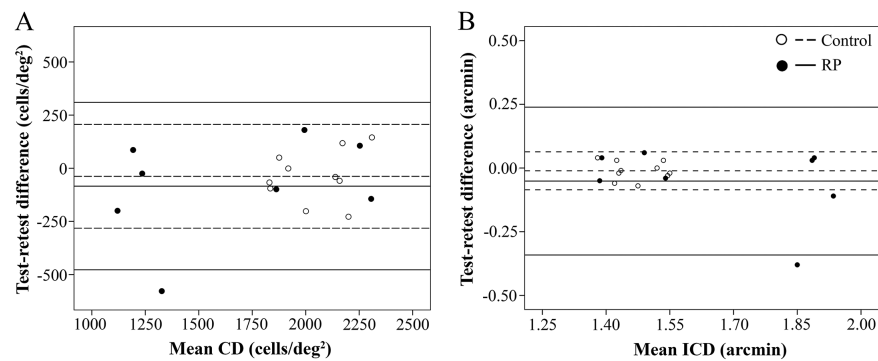


Figure 3. Bland–Altman plots show no relationship between intra-session test–retest difference and mean CD (**A**) and ICD (**B**) in the control and patient groups. In each eye, the two highest values from the same session were analyzed. For each group, the *middle, upper, and lower lines* represent mean +2 SD and –2 SD of the test–retest differences.

discarded due to inadequate image quality (Supplementary Fig. S4). At least two good-quality images were available for all eyes. The intra-session CoR of CD was 239 cells/deg² (2940 cells/mm²) in the control group, 468 cells/deg² (5649 cells/mm²) in the patient group at baseline, and 521 cells/deg² (6377 cells/mm²) at the 6-month follow-up (Table 3). The inter-session CoR of CD in the patient group was 560 cells/deg² (6654 cells/mm²). The intra-session CoR of ICD was 0.07 arcmin (0.35 μm) in the control group, 0.28 arcmin (1.37 μm) in the patient group at baseline, and 0.59 arcmin (2.89 μm) at the 6-month follow-up. The inter-session CoR of ICD in the patient group was 0.50 arcmin (2.40 μm). Details regarding the CoR values for ICD are shown in Supplementary Table S1. The Bland–Altman plot showed no significant relationship

between intra-session (Figs. 3A and 3B) and inter-session (Supplementary Figs. S5A and S5B) test-retest differences and mean CD or ICD in the control and patient groups.

Patterns of Cone Loss

The baseline mean parafoveal CD in the patient group was lower than that in the control group, but this difference was not statistically significant (1750 cells/deg² vs. 2094 cells/deg²; *P* = 0.09). CD was more than 2 SD less than the mean for the control group in four patients, including one patient with no EZ defect (Table 4). The baseline mean ICD values in the control and patient groups were 1.46 and

Table 4. Individual Baseline and Follow-Up EZ Span and CD in the Patient Group

ID	EZ Span, μm				CD, ^a Cells/deg ² (Cells/mm ²)			
	Baseline	6 Months	Change	Relative Change (%)	Baseline	6 Months	Change	Relative Change (%)
1	ND	ND	—	—	2306 (26,681)	2112 (24,436)	−194 (−2245)	−8.4 (8.4)
2	3275	3143	−132	−4.0	1912 (26,216)	1738 (23,828)	−174 (−2388)	−9.1 (9.1)
3	1392	1365	−27	−1.9	1236 (18,074)	1194 (17,469)	−42 (−605)	−3.4 (3.3)
4	ND	ND	—	—	1616 (19,135)	1198 (14,193)	−418 (−4942)	−25.9 (25.8)
5	2192	2146	−46	−2.1	1248 (10,919)	1055 (9227)	−193 (−1692)	−15.5 (15.5)
6	5558	5171	−387	−7.0	1220 (14,953)	1040 (12,746)	−180 (−2207)	−14.8 (14.8)
7	3604	3575	−29	−0.8	2378 (28,859)	2101 (25,493)	−277 (−3366)	−11.7 (11.7)
8	3113	2990	−123	−3.9	2084 (28,676)	1982 (27,276)	−102 (−1400)	−4.9 (4.9)
Mean	3189	3065	−124	−3.9	1750 (21,689)	1552 (19,333) ^b	−198 (−2356)	−11.3 (10.9)
SD	1416	1299	137	9.7	486 (6830)	478 (6790)	113 (1318)	23.2 (19.3)

ND, no defect within the SD-OCT horizontal B-scan imaging field (30°).

^aHighest CD among the four overlapping image frames.

^bStatistically significant compared with baseline ($P < 0.01$, paired-samples t -test).

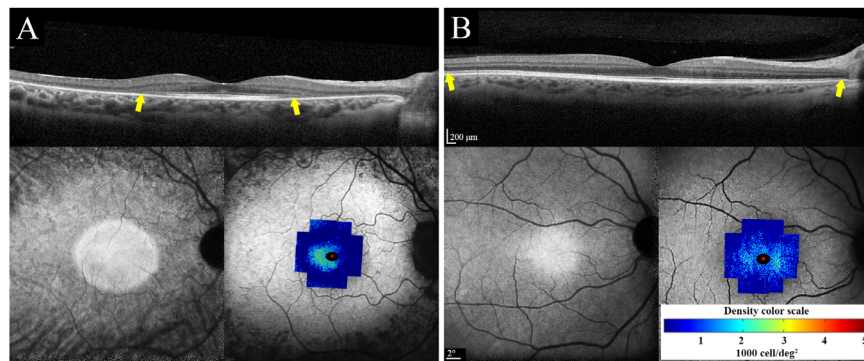


Figure 4. Macular SD-OCT (top), near-infrared autofluorescence (NI-AF; bottom left) and CD map overlaid on short-wavelength autofluorescence (SW-AF; bottom right) in two patients with RP. (A) Severe generalized cone loss with only preserved temporal cone mosaic in patient 8. (B) Severe perifoveal cone loss in patient 3 with autosomal recessive retinitis pigmentosa (ARRP). Ellipsoid zone appeared normal in areas with severe cone loss in both patients. Yellow arrows show the span of the ellipsoid zone, which was beyond the imaging field in patient 3. Scales of OCT, SW-AF, and CD are shown.

1.62 arcmin, respectively ($P = 0.08$). Details of individual ICDs are presented in Supplementary Table S2. A topographic map of the cone mosaic revealed different cone-loss patterns, including severe perifoveal cone loss and preserved temporal parafoveal cone mosaic (Fig. 4A), severe generalized cone loss in a patient with autosomal recessive retinitis pigmentosa (Fig. 4B), and mild perifoveal cone loss with preserved parafoveal cone mosaic in the patient with autosomal dominant retinitis pigmentosa (Fig. 5A). Severe cone loss was observed even in areas with normal EZ (Figs. 4A, 4B).

Longitudinal Cone Density Measurement

None of the patients developed new cataract, CME, or ERM during the follow-up period, and the mild cataract in patients 3 and 7 remained stable. Also, none of the patients developed ocular surface abnormality or pupil dilation defect at the follow-up examination. A trend toward decreasing CD over the 6-month follow-up was observed in all patients (Fig. 6). Mean CD declined from 1750 cells/deg² (21689 cells/mm²) at baseline to 1552 cells/deg² (19333 cells/mm²) at the 6-month follow-up (−198 cells/deg² or −11.3%;

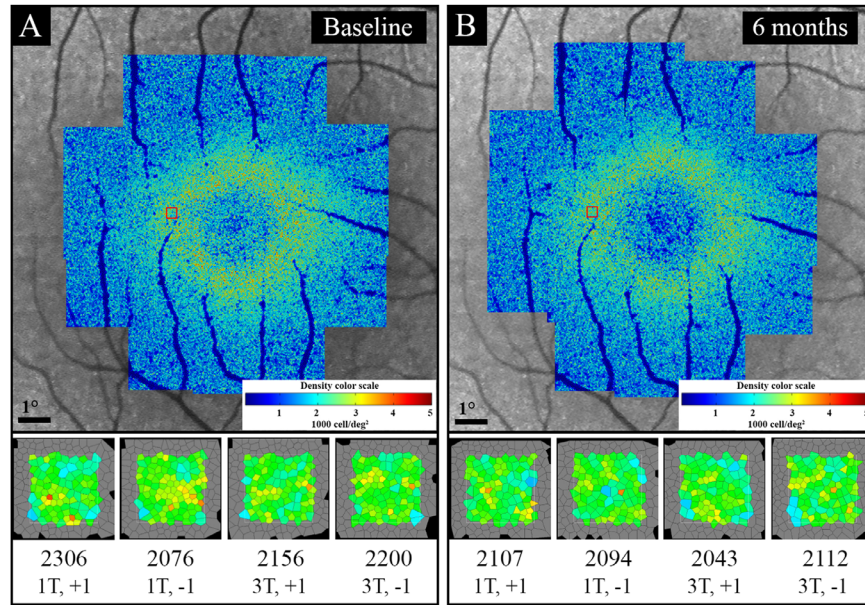


Figure 5. Example of baseline (A) and follow-up (B) CD map and analysis of ROI in four overlapping image frames in patient 1 with autosomal dominant retinitis pigmentosa (ADRP). There was an overall decline in parafoveal CD on the CD map at the 6-month follow-up (B) compared with baseline (A). Red boxes indicate the approximate location of the ROI. The bottom section shows a magnified image of the analyzed sampling window on each image frame, CD (cells/deg²; top line), and image frame centration coordinates (bottom line), showing a decline in CD at the 6-month follow-up (B) compared with baseline (A).

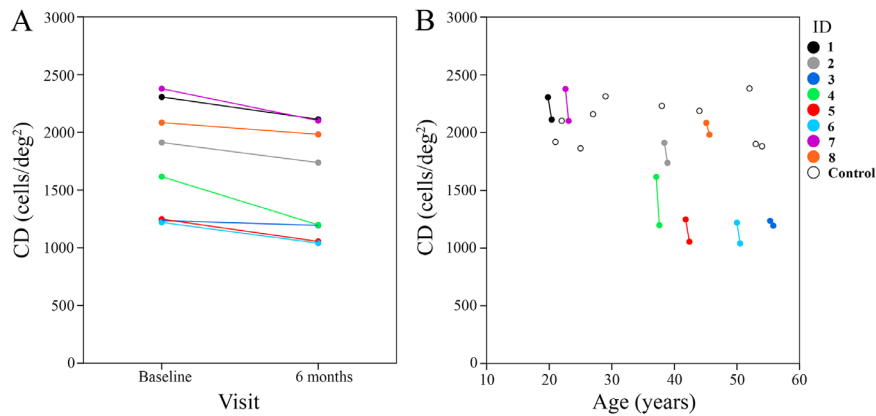


Figure 6. (A) CD declined between baseline and the 6-month follow-up. (B) Scatterplot of CD in control subjects superimposed on patients' baseline and follow-up measurements shows inter-individual variations across five decades of age range.

–2356 cells/mm² or –10.9%), which was statistically significant ($P < 0.01$ for both cells/deg² and cells/mm²) (Table 4, Fig. 6). ICD increased in seven patients and remained unchanged in the remaining patient. Mean ICD increased from 1.62 arcmin (7.79 μm) at baseline to 1.71 arcmin (8.23 μm) at the 6-month follow-up (0.09 arcmin or 5.5%; 0.45 μm or 5.6%), which was statistically significant ($P = 0.01$ for both arcmin and μm) (Supplementary Table S2). Although EZ span

declined in all patients with visible EZ endings ($n = 6$), the mean EZ decline at the 6-month follow-up was not statistically significant (3189 μm vs. 3065 μm, –3.9%; $P = 0.08$). Also, there was no significant difference between baseline and follow-up BCVA (logMAR) in the patient group (0.08 vs. 0.03; $P = 0.08$). Of interest, the two asymptomatic patients with no EZ defect revealed 8.4% and 25.9% loss of parafoveal CD at the 6-month follow-up (Table 4).

Discussion

Despite extensive investigations of cone mosaic changes in patients with IRDs using AOSLO and AOFIO,^{14,22,23} the repeatability and test–retest variability of these techniques have been addressed in few studies.^{15,24,25} In the only repeatability study using rtx1 in patients with RP, the inter-session CoR of CD at 2° eccentricity was 3514 cells/mm².¹⁷ In that report, the AO image center was used as the foveal center, which may differ from the actual anatomical foveal center and subsequently result in inaccurate localization of the ROI. In addition, that study used fully automated cone analysis software without manual adjustment, which may result in overestimation of CD.¹⁷ We found higher CoR values in patients with RCD. Unlike the aforementioned study, we aligned the AO montage with SD-OCT for better localization of the ROI and adjusted cone markings manually to minimize software errors in cone detection. In addition, we included ICD in our study, which supported a higher CoR in the patient group. The greater CoR observed in our patient group might be explained by differences in the imaging and image analysis protocols, criteria for exclusion of poor-quality images, and severity of disease in the studied sample. In addition, at least part of the intra-session variation in CD observed in our study may be due to the use of overlapping image frames with different fixation coordinates, which may induce variation in cone visualization through changes in wave-guiding properties. To overcome this limitation, we included the two image frames with the highest CD values and included ICD to minimize the rate and the impact of missing cones due to poor image quality and/or non-wave-guiding.

The resolution of AOFIO is insufficient to visualize foveal cones within the central 2° diameter and rods throughout the retina. In addition, cone visualization might be affected by the densely packed intervening rods beyond 6° from the fovea; hence, the usefulness of AOFIO is generally limited to eccentricities between 2° and 5°. ²⁰ Another limitation of the FIO technique is that image contrast may be compromised by light scattered from other retinal structures and choroid, especially at longer wavelengths.²⁶ This limitation can be overcome in non-commercial AO instruments by using split-detector (non-confocal) AOSLO, which resolves cone inner segments independent of reflectivity/waveguiding.²⁷

We observed a significant parafoveal cone loss in RCD patients, irrespective of the inheritance pattern and SD-OCT EZ span. We described different patterns of cone loss, which may be correlated with specific

genes in future studies on a larger and more diverse patient cohort. Identification and classification of patterns of parafoveal cone loss (e.g., presence of viable cones in atrophied outer retinal areas¹⁴) may have implications for genotype–phenotype correlation and treatment opportunities. To the best of our knowledge, longitudinal changes in cone mosaic using AOFIO in patients with RP have not been investigated previously. Talcott and colleagues²⁸ reported a 9% to 24% reduction in CD over 2-year follow-up in three eyes of three patients with RCD. In this proof-of-concept study, we reported a significant change in parafoveal CD and ICD at 6 months, suggesting a potential to shorten RCD clinical trials if this endpoint is used as the primary outcome. This contrasts with the use of SD-OCT EZ span, where a follow-up of at least 12 months was required to reach a significant change.⁸ The clinical relevance of our findings is dampened by the inconsistency in the acquisition of high AO image quality and the time-consuming process of semiautomated cone counting at matching retinal locations. Furthermore, there is still only limited information on how the changes in cone wave-guiding properties due to disease progression can be differentiated from physiological fluctuations over time.²⁹ Future studies are necessary to determine if the changes we observed at 6 months are predictive of eventual loss of EZ, retinal thickness, retinal sensitivity, and ultimately quality of life. Improved AO design and software capability are essential for overcoming the practical limitations imposed by ocular surface abnormalities (e.g., dry eye disease), media opacity (e.g., cataract), inner retinal abnormality (e.g., CME, ERM), and poor fixation.

Residual EZ span/area and thickness of the outer nuclear or photoreceptor layer have been used as structural outcome measures for monitoring the progression of RCD. Although SD-OCT is a feasible and reliable test for assessing the outer retinal structures, the resolution is not high enough to visualize individual photoreceptors. In addition, EZ span and layer thicknesses may not reveal subtle changes in patients with early-stage disease, as we demonstrated in two out of eight patients in our cohort. Gale et al.¹⁴ described cone mosaic changes using FIO in relation to SD-OCT findings in patients with RP and found normal cone mosaic in areas with preserved outer retinal layers; however, they did not perform quantitative cone mosaic analysis.¹⁴ In our study, parafoveal CD was lower than that in the control group, irrespective of the EZ span. In addition, a notable decline in CD was observed in the two patients with no attenuation of the EZ band within the imaging field. These findings suggest potential application of AO imaging in detecting ultrastructural abnormalities in RCD, before these

abnormalities become evident on SD-OCT. Future studies should incorporate dense raster volume scans over a larger field of view to enable *en face* reconstruction of the EZ band for calculation of EZ areas. In addition, we have not measured EZ reflectivity and thickness, which may reveal EZ attenuation prior to its shortening. Correlation among CD, ICD, and EZ integrity at the same retinal location may provide further insight into the utility of AO imaging in detecting disease progression.

The main limitation of our study was lack of repeated imaging at the same fixation coordinates to calculate short-term inter-session test–retest variability. We showed that a 6-month interval may be too long for this purpose, as CD and ICD showed significant differences with baseline. Instead, we analyzed four overlapping image frames and used the highest CD and the lowest ICD values for between-group comparisons and progression analysis. In addition, we analyzed cone mosaic on a single ROI, which may reduce the validity of our findings. More importantly, a large proportion of patients enrolled were not given the opportunity to have AO imaging or were excluded from the study due to low BCVA, significant cataract or history of cataract surgery, inner retinal abnormalities (i.e., CME and ERM), poor fixation, or a combination of these. Hence, our study design does not answer the question of whether AO imaging is useful clinically as a routine technique for monitoring RCD. Finally, our findings are limited by the small sample size and heterogeneous genotype and phenotypes. The progression data will be more useful and reliable using a genetically homogeneous sample. This was a proof-of-concept study to assess the capability of AO imaging in early detection of disease progression, rather than a definitive study that provides an estimate of cone loss rate using AO imaging. The latter will require multiple imaging sessions and longer follow-up duration in a genetically homogeneous sample. Our study emphasizes the usefulness of AO imaging in future RP trials. Future studies to address the feasibility and utility of AO imaging will require a prospective design that includes patients with the same genotype, preferably in the early stages of the disease, to ensure continuity in linking changes in wave-guiding properties of the cones with gross changes in SD-OCT and microperimetry.

Conclusions

We report, for the first time, longitudinal parafoveal CD and ICD changes assessed using a commercial

AOFIO camera and software in patients with RCD. We have highlighted concerns regarding using montage images to analyze cone mosaic parameters in ROIs shared by image frames centered at different coordinates. We also showed that parafoveal CD and ICD may be used as potential structural endpoints in eligible patients, especially those with early-stage disease who have not developed complications such as cataract and severe outer retinal atrophy. The use of AO imaging may be limited to natural history studies in early-stage RP at this stage. However, evolution of photoreceptor rescue strategies that facilitate early intervention may expand the use of AO imaging to clinical trials in the future. Further studies are required to validate our results by studying the test–retest variability of serial CD and ICD measurements.

Acknowledgments

The authors thank the participants and their families, as well as Amanda Scurry and Jayme Glynn for their assistance in organizing the patient appointments for the clinical assessments.

Supported by grants from the Australian National Health and Medical Research Council (GNT116360, GNT1188694, GNT1054712, and MRF1142962 to FKC), by the McCusker Charitable Foundation (JC), by a Mioceovich Retina Fellowship (RCHJ), and by a UWA Postgraduate Research Scholarship (DR). The sponsor or funding organization had no role in the design or conduct of this research.

Disclosure: **D. Roshandel**, None; **R.C. Heath Jeffery**, None; **J. Charng**, None; **D.M. Sampson**, None; **S. McLenachan**, None; **D.A. Mackey**, None; **F.K. Chen**, None

References

1. Roshandel D, Thompson JA, Charng J, et al. Exploring microperimetry and autofluorescence endpoints for monitoring disease progression in PRPF31-associated retinopathy. *Ophthalmic Genet.* 2020;42:1–14.
2. Cehajic-Kapetanovic J, Xue K, Martinez-Fernandez de la Camara C, et al. Initial results from a first-in-human gene therapy trial on X-linked retinitis pigmentosa caused by mutations in RPGR. *Nat Med.* 2020;26:354–359.

3. Ramachandran R, Zhou L, Locke KG, Birch DG, Hood DC. A comparison of methods for tracking progression in X-linked retinitis pigmentosa using frequency domain OCT. *Transl Vis Sci Technol.* 2013;2:5.
4. Birch DG, Locke KG, Wen Y, Locke KI, Hoffman DR, Hood DC. Spectral-domain optical coherence tomography measures of outer segment layer progression in patients with X-linked retinitis pigmentosa. *JAMA Ophthalmol.* 2013;131:1143–1150.
5. Cai CX, Locke KG, Ramachandran R, Birch DG, Hood DC. A comparison of progressive loss of the ellipsoid zone (EZ) band in autosomal dominant and x-linked retinitis pigmentosa. *Invest Ophthalmol Vis Sci.* 2014;55:7417–7422.
6. Colombo L, Montesano G, Sala B, et al. Comparison of 5-year progression of retinitis pigmentosa involving the posterior pole among siblings by means of SD-OCT: a retrospective study. *BMC Ophthalmol.* 2018;18:153.
7. Hariri AH, Zhang HY, Ho A, et al. Quantification of ellipsoid zone changes in retinitis pigmentosa using en face spectral domain–optical coherence tomography. *JAMA Ophthalmol.* 2016;134:628–635.
8. Calzetti G, Levy RA, Cideciyan AV, et al. Efficacy outcome measures for clinical trials of USH2A caused by the common c.2299delG mutation. *Am J Ophthalmol.* 2018;193:114–129.
9. Zhang B, Li N, Kang J, He Y, Chen X-M. Adaptive optics scanning laser ophthalmoscopy in fundus imaging, a review and update. *Int J Ophthalmol.* 2017;10:1751.
10. Tumahai P, Moureaux C, Meillat M, et al. High-resolution imaging of photoreceptors in healthy human eyes using an adaptive optics retinal camera. *Eye (Lond).* 2018;32:1723–1730.
11. Chui TY, Song H, Burns SA. Adaptive-optics imaging of human cone photoreceptor distribution. *J Opt Soc Am A Opt Image Sci Vis.* 2008;25:3021–3029.
12. Legras R, Gaudric A, Woog K. Distribution of cone density, spacing and arrangement in adult healthy retinas with adaptive optics flood illumination. *PLoS One.* 2018;13:e0191141.
13. Duncan JL, Zhang Y, Gandhi J, et al. High-resolution imaging with adaptive optics in patients with inherited retinal degeneration. *Invest Ophthalmol Vis Sci.* 2007;48:3283–3291.
14. Gale MJ, Feng S, Titus HE, Smith TB, Pennesi ME. Interpretation of flood-illuminated adaptive optics images in subjects with retinitis pigmentosa. *Adv Exp Med Biol.* 2016;854:291–297.
15. Tanna P, Kasilian M, Strauss R, et al. Reliability and repeatability of cone density measurements in patients with Stargardt disease and RPGR-associated retinopathy. *Invest Ophthalmol Vis Sci.* 2017;58:3608–3615.
16. Tojo N, Nakamura T, Fuchizawa C, Oiwake T, Hayashi A. Adaptive optics fundus images of cone photoreceptors in the macula of patients with retinitis pigmentosa. *Clin Ophthalmol.* 2013;7:203–210.
17. Gale MJ, Harman GA, Chen J, Pennesi ME. Repeatability of adaptive optics automated cone measurements in subjects with retinitis pigmentosa and novel metrics for assessment of image quality. *Transl Vis Sci Technol.* 2019;8:17.
18. Feng S, Gale MJ, Fay JD, et al. Assessment of different sampling methods for measuring and representing macular cone density using flood-illuminated adaptive optics. *Invest Ophthalmol Vis Sci.* 2015;56:5751–5763.
19. Chen FK, Agelis LE, Peh KK, Teong J, Wong ENXM. Factors contributing to discrepancy between visual acuity fractions derived from a Snellen chart and letter scores on the early treatment diabetic retinopathy study chart. *Asia Pac J Ophthalmol.* 2014;3:277–285.
20. Muthiah MN, Gias C, Chen FK, et al. Cone photoreceptor definition on adaptive optics retinal imaging. *Br J Ophthalmol.* 2014;98:1073–1079.
21. Garrioch R, Langlo C, Dubis AM, Cooper RF, Dubra A, Carroll J. Repeatability of in vivo parafoveal cone density and spacing measurements. *Optom Vis Sci.* 2012;89:632–643.
22. Ueno S, Koyanagi Y, Kominami T, et al. Clinical characteristics and high resolution retinal imaging of retinitis pigmentosa caused by RP1 gene variants. *Jpn J Ophthalmol.* 2020;64:485–496.
23. Kubota D, Matsumoto K, Hayashi M, et al. High-resolution photoreceptor imaging analysis of patients with autosomal dominant retinitis pigmentosa (ADRP) caused by HK1 mutation. *Ophthalmic Genet.* 2020;41:629–638.
24. Zayit-Soudry S, Sippl-Swezey N, Porco TC, et al. Repeatability of cone spacing measures in eyes with inherited retinal degenerations. *Invest Ophthalmol Vis Sci.* 2015;56:6179–6189.
25. Sun LW, Johnson RD, Langlo CS, et al. Assessing photoreceptor structure in retinitis pigmentosa and Usher syndrome. *Invest Ophthalmol Vis Sci.* 2016;57:2428–2442.
26. Burns SA, Elsner AE, Sapoznik KA, Warner RL, Gast TJ. Adaptive optics imaging of the human retina. *Prog Retin Eye Res.* 2019;68:1–30.

27. Scoles D, Sulai YN, Langlo CS, et al. In vivo imaging of human cone photoreceptor inner segments. *Invest Ophthalmol Vis Sci.* 2014;55:4244–4251.
28. Talcott KE, Ratnam K, Sundquist SM, et al. Longitudinal study of cone photoreceptors during retinal degeneration and in response to ciliary neurotrophic factor treatment. *Invest Ophthalmol Vis Sci.* 2011;52:2219–2226.
29. Mariotti L, Devaney N, Lombardo G, Lombardo M. Understanding the changes of cone reflectance in adaptive optics flood illumination retinal images over three years. *Biomed Opt Express.* 2016;7:2807–2822.